Crack mode and life of Ti-6Al-4V under multiaxial low cycle fatigue

Takamoto Itoh, Masao Sakane
Department of Mechanical Engineering, College of Science & Engineering, Ritsumeikan University, Japan
itohtaka@fc.ritsumei.ac.jp, sakanem@se.ritsumei.ac.jp

Takahiro Morishita
Graduate School of Science & Engineering, Ritsumeikan University, Japan
gr0202xp@ed.ritsumei.ac.jp

Hiroshi Nakamura
Engine Technology Department, Aero-Engine & Space Operation, IHI Corporation, Japan
hiroshi_nakamura_2@ihi.co.jp

Masahiro Takanashi
Structural Strength Department, Research Laboratory, IHI Corporation, Japan
masahiro_takanashi@ihi.co.jp

ABSTRACT. This paper studies multiaxial low cycle fatigue crack mode and failure life of Ti-6Al-4V. Stress controlled fatigue tests were carried out using a hollow cylinder specimen under multiaxial loadings of λ=0, 0.4, 0.5 and 1 of which stress ratio R=0 at room temperature. λ is a principal stress ratio and is defined as $\lambda = \sigma_{II}/\sigma_I$, where σ_I and σ_{II} are principal stresses of which absolute values take the largest and middle ones, respectively. Here, the test at λ=0 is a uniaxial loading test and that at λ=1 an equi-biaxial loading test. A testing machine employed is a newly developed multiaxial fatigue testing machine which can apply push-pull and reversed torsion loadings with inner pressure onto the hollow cylinder specimen. Based on the obtained results, this study discusses evaluation of the biaxial low cycle fatigue life and crack mode. Failure life is reduced with increasing λ induced by cyclic ratcheting. The crack mode is affected by the surface condition of cut-machining and the failure life depends on the crack mode in the multiaxial loading largely.

KEYWORDS. Ti-6Al-4V; Low cycle fatigue; Multiaxial loading; Crack mode; Hollow cylinder specimen; Inner pressure

INTRODUCTION

T i-6Al-4V is frequently used as a material in rotating aero engines because it has the properties of high strength, light weight, and excellent corrosion resistance. A rotating aero engine receives cyclic loading under thermal and mechanical stresses which cause multiaxial low cycle fatigue. Under non-proportional loading in which the

principal directions of stress and strain are changed cyclically, previous studies have reported a drastic reduction in the failure life with accompanying additional cyclic hardening [1-16] depending on both the loading path and the material [6, 8, 10, 13, 16]. In addition, some studies about the fatigue property of Ti alloys have been reported [17, 18]. Meanwhile, only a paper by the authors [19] has dealt with multiaxial low cycle fatigue crack behavior of Ti-6Al-4V.

To evaluate fatigue lives under multiaxial loading conditions, multiaxial fatigue models which relate fatigue lives to uniaxial fatigue properties have been established. Equivalent strains and stresses based on the theories of von Mises and Tresca, which are considered the most commonly used theory, but lead to significant overestimation of fatigue lives under non-proportional loadings from those under proportional loading. Therefore, other life evaluation models have been proposed such as critical plane approaches; i) Stress based critical plane approaches presented by Findley [20] and McDiarmid [21], ii) Strain based critical plane approach by Brown and Miller [22] and Wang and Brown [23], iii) Strain-stress based critical plane approaches by Fatemi and Socie [7, 15] and Smith, Watson and Topper [24]. Most of these models are success on life evaluation under non-proportional loadings, however, some of them have some limitation on application. Itoh *et al.* [8, 10, 13, 16] proposed a strain parameter taking into account the loading path and material dependencies of life, which shows good correlations with lives under non-proportional loadings for different materials [16]. The studies mentioned above treat the fatigue properties under limited multiaxial loadings of which the principal stress ratio λ range is −1≤λ (=σ_{II}/σ_I)≤0, where σ_I is the principal stress whose absolute value is the maximum and σ_{II} one of which absolute value the middle. The reason why the performable principal stress ratio range was limited to −1≤λ≤0 mainly due to the testing method to apply the axial and twist loads to hollow cylinder specimens. However, to carry out the multiaxial fatigue test beyond the principal stress ratio range, special multiaxial fatigue testing stands must be required. The authors developed a new testing machine which can apply push-pull and reversed torsion loadings and additionally inner pressure onto the hollow cylinder specimen to perform the test in −1≤λ≤1 under proportional and non-proportional loadings.

In this study, biaxial fatigue tests of the stress ratio range 0≤λ≤1 were carried out using the hollow cylinder specimen of Ti-6Al-4V by the developed multiaxial fatigue testing machine and properties of failure life and crack mode are discussed.

MULTIAXIAL LOADING AND TESTING MACHINE

Definition of stress and strain multiaxiality

Multiaxial stress and strain states can be expressed by using parameters, ϰ and φ which are the stress and the strain ratios, as equated in Eq. (1) and Eq. (2),

$$\kappa = \frac{\tau}{\sigma} \tag{1}$$

$$\phi = \frac{\gamma}{\varepsilon} \tag{2}$$

where σ and τ are axial and shear stresses and ε and γ are axial and shear strains in plane stress state.

Besides the method above, this paper also employs principal stress ratio, λ, and the principal strain ratio, φ, to define multiaxial stress and strain states, which are equated in Eq. (3) and Eq. (4),

$$\lambda = \frac{\sigma_{II}}{\sigma_I} \tag{3}$$

$$\varphi = \frac{\varepsilon_{II}}{\varepsilon_I} \tag{4}$$

where σ_I and σ_{II} are put as principal stresses, σ_1, σ_2 or σ_3 ($\sigma_1 \geq \sigma_2 \geq \sigma_3$) of which absolute values takes the largest and middle ones, *e.g.*, if σ_1=100MP, σ_2=50MP and σ_3=−200MP, σ_I=−200MPa and σ_{II}=100MPa since $|\sigma_3| \geq |\sigma_1| \geq |\sigma_2|$. On the other hand, ε_I and ε_{II} are principal strains of which principal direction corresponding to those of σ_I and σ_{II},

respectively. In proportional fatigue test, λ and ϕ have constant values in a cycle. For tension-compression tests using the hollow cylinder specimen, relationships among σ_1, σ_3, σ, τ and ε_1, ε_3, ε, γ are shown in Eq. (5) and Eq. (6).

$$\left.\begin{array}{c}\sigma_1 \\ \sigma_3\end{array}\right\} = \frac{\sigma}{2} \pm \frac{1}{2}\sqrt{\sigma^2 + 4\tau^2} \tag{5}$$

$$\left.\begin{array}{c}\varepsilon_1 \\ \varepsilon_3\end{array}\right\} = \left(\frac{1-\nu}{2}\right)\varepsilon \pm \frac{1}{2}\sqrt{(1+\nu)^2\,\varepsilon^2 + \gamma^2} \tag{6}$$

In Eq. (6), ν is the Poisson's ratio. Usually, the value of Poisson's ratio is around 0.3 in elastic regime but it is 0.5 in a fully plastic regime.

Uniaxial and multiaxial stress and strain states

A stress state is defined as multiaxial state if the multiple principal stresses operate and a strain state as multiaxial state when the multiple principal strains do. Using these definitions, the multiaxial stress state does not always correspond to the multiaxial strain state. For example, Fig. 1, an uniaxial tension loading is the uniaxial stress state because only one principal stress operates in tensile direction but this case becomes the multiaxial strain state because the two additional principal strains are caused by the lateral contraction as well as the tensile direction. These definitions of multiaxiality are most consistent for describing the multiaxial stress and strain states compared to using the other stress and strain components, whereas stress multiaxiality does not always correspond to strain multiaxiality.

Non-proportional loading is defined as the loading where the directions of the principal stresses or strains rotate, and proportional loading when they are fixed.
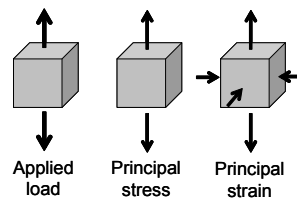

Figure 1: Principal stress and principal strain in tension loading.

Figure 2: Applied stresses/strains and stress/strain multiaxiality in proportional loading. (a) Stress state, (b) Strain state.

Proportional loading

Figs. 2 (a) and (b) summarize the applied stresses/strains and the stress/strain multiaxiality in various proportional multiaxial testing methods under the plane stress condition. In the tension-compression test, a uniaxial stress (σ) is applied

to the specimen in Fig. 2 (a) and a uniaxial strain (ε) is applied to the specimen but the multiple principal strains arise in the specimen thickness direction in Fig. 2 (b). The lateral strain is $-\nu\varepsilon$ is applied to the specimen. In the reversed torsion test, the applied stress/strain is only the shear stress/stress (τ/γ) but the two principal stresses/strains with the opposite sign are caused in this case. So, the reversed torsion test also becomes a multiaxial test. The combined tension-torsion and the biaxial tension-compression loadings also enable the fatigue test in multiaxial strain states. The former test only covers the stress/strain biaxiality for $-1\leq\lambda\leq0/-1\leq\phi\leq-\nu$ but the latter test does $-1\leq\lambda, \phi\leq1$.

Non-proportional loading
Fig. 3 shows the tension-compression and reversed torsion testing and the biaxial tension-compression testing with phase shift in applied strains. In the tension-torsion test with the phase shift, the direction of the principal strains rotates with time and this loading is non-proportional loading. The phase shift in applied strain in the biaxial tension-compression test causes no rotation of the principal strains but it causes the switch of the principal strain directions. The authors consider that this loading should be classified to a proportional loading because no large additional hardening and little reduction of fatigue life was confirmed in this type of test using type 304 steel cruciform specimens at 823 K [12]. However, another research [25] stated that this loading should be a type of non-proportional tests showing a fair reduction of fatigue lives in experiments. More detailed experimental studies and evidences are needed to have a definite conclusion on the classification of this type of loading.

Figure 3: Definition of non-proportional loading.

Figure 4: Type of specimens.

Types of multiaxial fatigue tests
Fig. 4 shows four types of common used multiaxial fatigue testing methods classified by types of loading and specimen. Type IA is the tension-compression and reversed torsion test using the hollow cylinder specimen, which is most widely used testing. Type IB is similar to Type IA from the point of using the hollow cylinder specimen but Type IB is applied with the internal and external pressures in addition to the tension-compression and reversed torsion loadings. Type II is the biaxial tension-compression testing using the cruciform specimen. Type III is the tri-axial tension-compression testing using a cubic specimen.
Principal stain and stress ratio ranges which can be performed in each type of test are summarized here. Type IA have been used widely multiaxial fatigue studies, but the principal stress/strain ratio range performable by this testing is $-1<\lambda\leq0/-1<\phi\leq-\nu$. Types IB and II can perform the multiaxial fatigue test under full ranged principal stress/strain ratio range of $-1<\lambda, \phi\leq1$. Type III also does the test under the same multiaxial strain state and tri-axial tension-compression loading, too. However, Types II and III have no change in principal directions of stress and strain since the directions always fixed into the direction of applied loading. Only type IB can perform the multiaxial fatigue test in the full ranged principal stress/strain ratio range with non-proportional loading.

Multiaxial fatigue testing machine for tension-torsion and inner pressure
Fig. 5 (a) shows a schematic view of the testing machine used in this study of which type is corresponds to Type IB. To generate the inner pressure with tension and torsion loadings, additional hydraulic actuators is installed into the common

used push-pull and reversed torsion testing machine. For measurements of axial, torsional and hoop strains, inductive displacement sensor type extensometers are mounted directly onto the specimen. To measure and evaluate axial, torsional and hoop stresses, load cells for axial load and torque and pressure gauge are installed. The maximum loads are ±50kN for push-pull and ±250N·m for torsion and the maximum inner pressures is 200MPa. By applying these loads, this testing machine can perform the multiaxial fatigue tests under the principal stress ratio range of −1≤λ≤1.

Test control system of this testing machine becomes more complicated than those in common used testing machines since three hydraulic actuators must be controlled simultaneously and independently by employing a test controller program and a system as shown in Fig. 5 (b). In order to raise the precision of control, three types of feedback (FB) loop are applied in this testing machine. First one is from load cell to servo amplifier for axial and torsional control, which operates on load-controlled mode. Second one is from strain gauge to servo amplifier for axial and torsional control, which operates on displacement-controlled mode. The load or the displacement control can be changed by FB selection switch. The last one is from pressure gauge to servo amplifier to control the inner pressure as test control programed.

The specimen employed is the hollow cylinder specimens designed for this testing machine of which shapes and dimensions will be shown later.
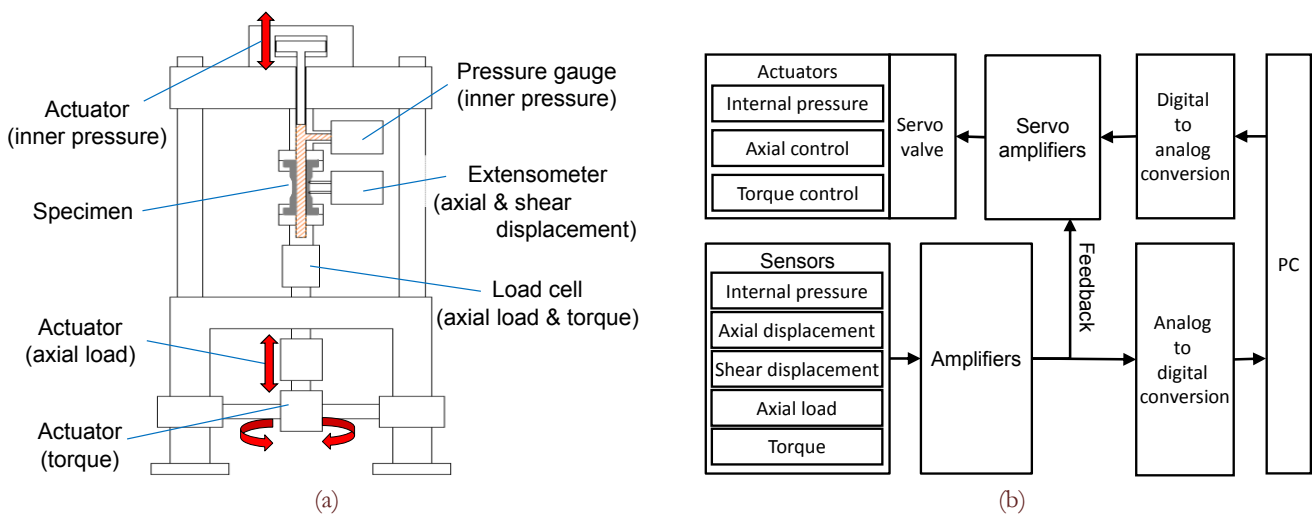

Figure 5: Multiaxial testing machine for push-pull, reversed torsion and inner pressure. (a) Schematic showing of multiaxial testing machine, (b) Over view of control system.

TEST MATERIAL AND EXPERIMENTAL PROCEDURE

The material tested was Ti-6Al-4V, which was subject to solution treatment at 960°C for 1 hour followed by water cooling, annealing at 705°C for 2 hours and air cooling. Fig. 6 shows the micro structure, which consists of alpha phases (hexagonal close-packed crystal structure) and the dual alpha- and beta-phase mixture (body-centered cubic crystal structure).
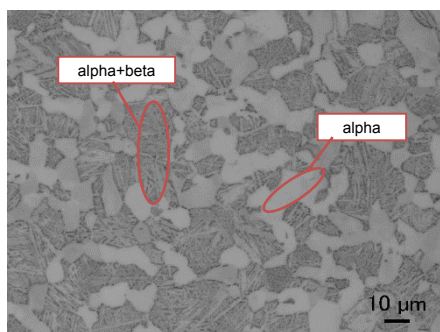

Figure 6: Microstructure of Ti-6Al-4V alloy.

Fig. 7 shows the shape and dimensions of hollow cylinder specimen employed which has a 12 mm inner diameter, a 14 mm outer diameter, and an 8.5 mm parallel at gauge part. In the figure, a coordinate employed are indicated with principal stresses. σ_1 is the maximum principal stress, σ_2 is the middle principal stress. In this test, σ_1 and σ_2 are equivalent to axial stress σ_z and hoop stress σ_θ equated by the following equations,

$$\sigma_1 = \sigma_z = \frac{F}{\frac{\pi}{4}\left(D_o^2 - D_i^2\right)} + \frac{P \cdot \frac{\pi}{4}\left(D_i^2\right)}{\frac{\pi}{4}\left(D_o^2 - D_i^2\right)} \tag{7}$$

$$\sigma_2 = \sigma_\theta = \frac{P \cdot D_i}{D_o - D_i} \tag{8}$$

where F and P are axial load and inner pressure, respectively. D_i and D_o are inner and outer diameters at gauge part of the specimen.
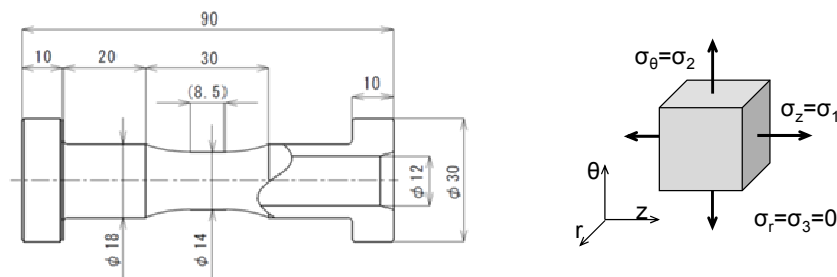

Figure 7: Shape and dimensions of test specimens (mm) with coordinate.

Stress controlled low cycle fatigue tests with proportional zero-peak loading were conducted under 4 types of stress paths shown in Fig. 8. In the figure, each stress path takes the principal stress ratio, λ=0, 0.4, 0.5 and 1.0. The dashed line shows a constant Mises' equivalent stress at 800 MPa. In the test at λ=0.4, peak stress was set at 858 MPa. The other λ's test at 800 MPa.
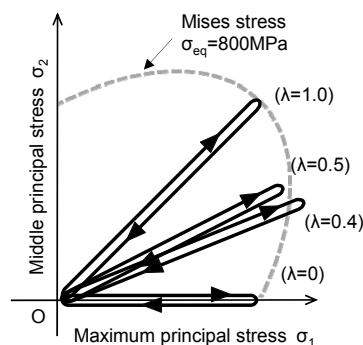

Figure 8: Principal stress path.

Fig. 9 shows strain waveforms of axial load (F), inner pressure (P) and axial stress (σ_z), hoop stress (σ_θ). Test frequencies in the uniaxial fatigue test (λ=0) and the biaxial fatigue tests (λ=0.4, 0.5, 1.0) are 0.4 Hz and 0.2 Hz, respectively. Number of cycles to failure (failure life), N_f, was determined as the cycle at which the maximum inner pressure was reduced due to leak of oil by initiation of through crack or rupture of the specimen.

Tab. 1 summarizes test conditions conducted. In the table, $\sigma_{z\,max}$ and $\sigma_{\theta\,max}$ are maximum values of σ_z and σ_θ obtained at the peak load, respectively. $\sigma_{eq\,max}$ a maximum value of Mises' equivalent stress (σ_{eq}) equated by

$$\sigma_{eq} = \frac{1}{2}\sqrt{\left(\sigma_r\right)^2 + \left(\sigma_\theta\right)^2 + \left(\sigma_r - \sigma_\theta\right)^2} \tag{9}$$

The inner and outer surfaces at the gauge part of the specimen were ground to an averaged surface roughness 1.6μm by honing machine. After the honing, some specimen were also received polishing and buffing to 10μm Al_2O_3 denoted by 'Polish' in Tab. 1.
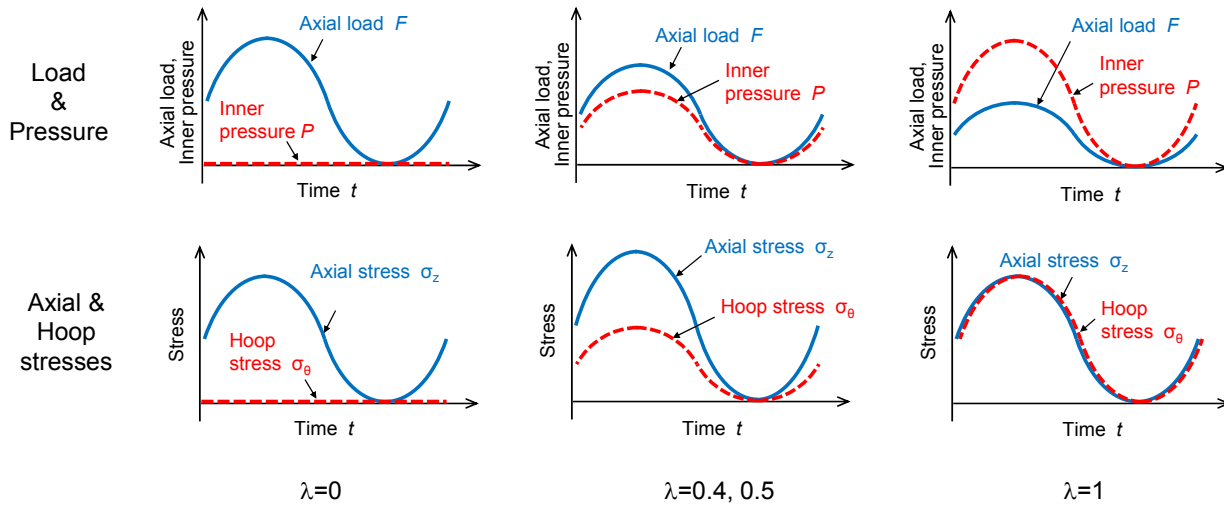

Figure 9: Wave forms of axial load, inner pressure, axial and hoop stresses.

Stress path		Maximum stress (MPa)			Polish/ Non-polish
Uniaxial/Biaxial	λ	Axial stress $\sigma_{z\,max}$	Hoop stress $\sigma_{\theta\,max}$	Mises stress $\sigma_{eq\,max}$	
Uniaxial Fatigue	0	800	—	800	Non-polish Polish
Biaxial Fatigue	0.4	985	400	858	Non-polish Polish
	0.5	924	462	800	Polish
	1.0	800	800	800	Polish

Table 1: List of fatigue test condition.

EXPERIMENTAL RESULTS AND DISCUSSION

Failure life

Fig. 10 shows a comparison of failure lives. In this figure, failure lives are normalized by the mean value of failure life in the uniaxial fatigue tests (λ=0 tests) tested using polished and non-polished specimens. In comparing the failure lives tested using the polished specimen, failure lives (N_f) tend to decrease with increase of the principal stress ratio (λ) although N_f at λ=0.4 is slightly shorter than N_f at λ=0.5. The shorter life in the λ=0.4 test may come from that the maximum Mises' equivalent stress in the test is slightly larger than those in the other λ's tests as shown in Tab. 1. The specimen polishing effect can be seen in the λ=0 and λ=0.4 tests. In the λ=0 test, N_f with non-polished specimen have longer life by about 20 % than that with polished specimen. In the λ=0.4 test, conversely, N_f with non-polished specimen is shorter than that with the polished specimen and the reduction ratio is down to approximately 50 % depending on each specimen.

The effects of λ and polishing on the failure life will be discussed in following sections.
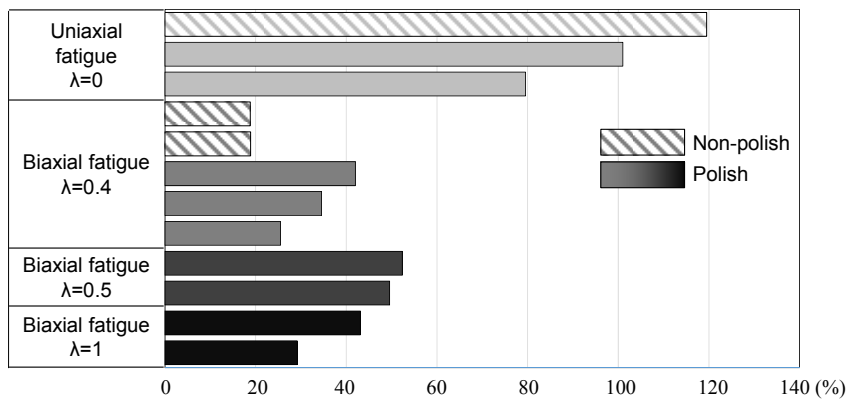
Figure 10: Comparison of failure lives at each principal stress ratio's test.

Dependence of defamation behavior on multiaxiality

Fig. 11 shows variation of mean axial strain ($\varepsilon_{z\,mean}$) as a function of cycle (N). In the figure, the vertical axis is normalized by mean axial strain at 10 cycles ($\varepsilon_{z\,mean10}$) and the horizontal normalized by (N/N_f). In all the tests, mean strains increase gradually with increase of cycles, *i.e.*, cyclic ratcheting occurs because the stress amplitude employed was relative high comparing with the yield stress 113 GPa. The degree of the ratcheting becomes larger with increasing λ and the larger ratcheting may leads to the reduction in failure life.

In structural components using Ti-6Al-4V, on the other hand, the stress level under service loadings is usually much lower than that employed in this study. In this case, no or small ratcheting will occur resulting in smaller effect of λ on failure life. However, the property of failure life under multiaxial loading at lower stress levels is still open question and additional experimental tests at the stress revel are required to confirm them.
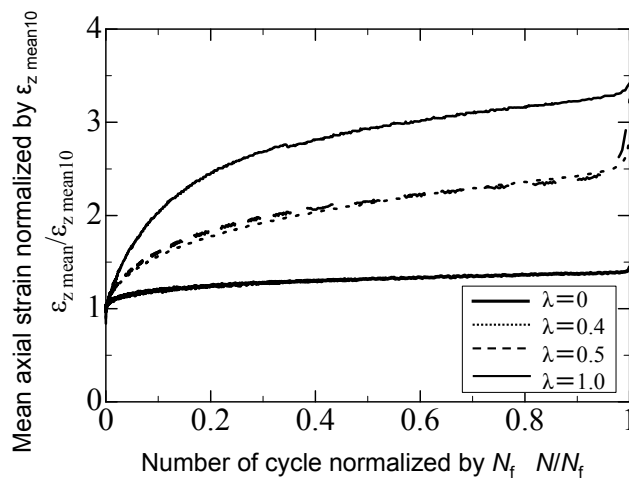

Figure 11: Variation of mean axial strains at each principal stress ratio's test.

Surface crack and effects polishing on failure life

Fig. 12 shows cracks observed on specimen surface fatigued at each λ's test. In the figure, the upper side shows surface cracks observed by optical microscope and the lower side schematic showings of the main crack.

Using the polished specimen, the crack in the $\lambda=0$ test shows a zigzag shape crack. Each zigzag crack is approximately 100 μm in length and has propagation directions of ±45 degrees from the specimen axial direction and then the macro-crack formed by linking of each zigzag crack propagated normal to the axial direction. In the tests at $\lambda=0.4$ and 0.5, observed cracks are similar to that at $\lambda=0$ although length of each zigzag crack is slightly smaller. In the $\lambda=1.0$ test, a main crack is observed in the direction of specimen axis and small cracks are also observed around the main crack in various direction.

Using the non-polished specimen, on the other hand, the crack at $\lambda=0$ test is slightly different from that at $\lambda=0$ test with the polished specimen. The crack shows the zigzag one but it may be formed by linking cracks propagating along cutting

scratches yielded in machining. In the λ=0.4 test with the non-polishing specimen, a straight crack is observed propagating along the cutting scratch.

Fig. 13 shows Mohr's stress circles and principal shear stress planes with normal and shear stresses on their planes in each λ state. At λ=0, the equivalent maximum shear stresses planes exists on planes normal and 45 degree incline to free surfaces. These two planes intersect with the surface plane in directions of 45 degree and normal to the specimen axis, respectively. So there are two possibilities of crack propagation which may results in the different crack mode between polish and non-polish specimens. In the λ=0.4 test, the maximum shear stress plane is 45 degree incline to the free surface on which normal and shear stresses are 493 MPa. The second principal shear stress plane is normal to the free surface of which normal and shear stresses are 693MPa and 293MPa, respectively. On this plane, the shear stress is much smaller but the normal stress is larger than those on the maximum shear stress plane. Comparing the equivalent Mises' stresses on these planes, the values have a small difference, 985MPa on the maximum shear stress plane and 858MPa on the second principal shear stress plane, which may suggests that which plane cracks propagate is undecidable depending on specimen surface condition.

The crack mode may be affected by the specimen surface condition in uniaxial and biaxial fatigue tests and the difference in the crack mode has a possibility affecting on failure lives largely in the biaxial fatigue tests. However, more detail crack observation and discussion will be required about the crack modes in biaxial stress condition.
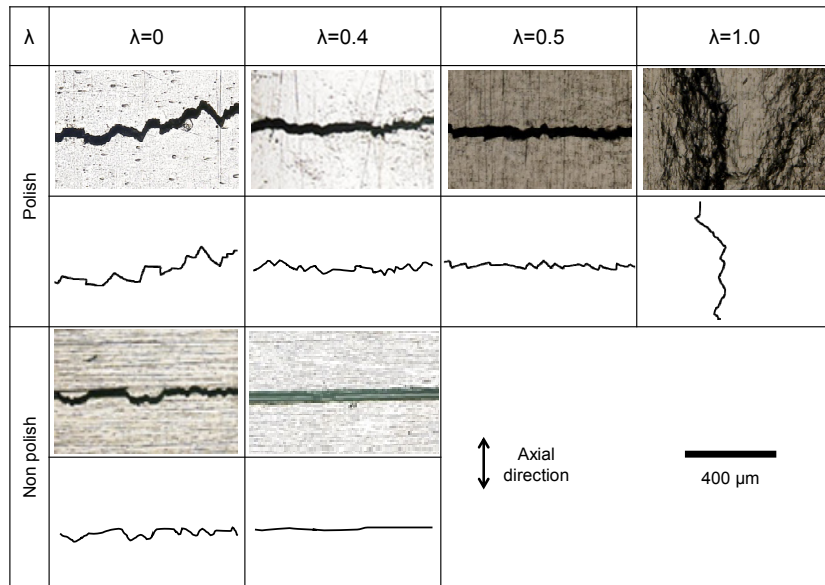

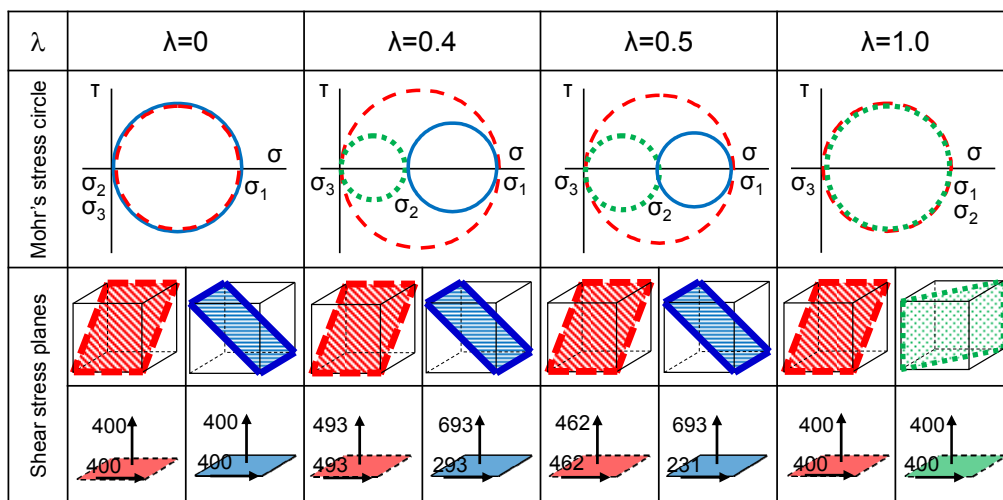Figure 12: Main crack shape on the surface of specimen.

Figure 13: Mohr's stress circle and maximum shear plane in principal stress ratio.

CONCLUSIONS

1. Multiaxial failure lives of Ti-6Al-4V depend on multiaxiality and decrease with increase of principal stress ratio, λ. The reduction is caused by cyclic ratcheting.
2. Crack mode at each λ's test depends on specimen surface condition of machining. In biaxial loading test, failure life is affected by the crack mode.

REFERENCES

[1] Kanazawa, K., Miller, K.J., Brown M.W., Cyclic deformation of 1%Cr-Mo-V steel under out-of-phase loads. Fatigue Eng Mater Struct, 2(3) (1979) 217–228.

[2] McDowell, F.L., On the path dependence of transient hardening and softening to stable states under complex biaxial cyclic loading. In: Desai and Gallagher, editors. Proc int conf constitutive laws eng mater, (1983) 125-135.

[3] Krempl, E., Lu, H., Comparison of the stress response of an aluminum alloy tube to proportional and alternate axial and shear strain paths at room temperature. Mechanics of Materials, 2(3) (1983) 183–192.

[4] Socie, D.F., Multiaxial fatigue damage models. Trans Am Soc Mech Eng – J Eng Mater Technol, 109(4) (1987) 293–298.

[5] Nitta, A., Ogata, T., Kuwabara, K., The effect of axial-torsional straining phase on elevated-temperature biaxial low-cycle fatigue life in SUS304 stainless steel. J Soc Mater Sci Jpn,. 36(403) (1987) 376–382.

[6] Doong, S.H., Socie, D.F., Robertson, I.M., Dislocation substructures and nonproportional hardening. Trans Am Soc Mech Eng – J Eng Mater Technol, 112(4) (1987)456–465.

[7] Fatemi, A., Socie, D.F., A critical plane approach to multiaxial fatigue damage including out-of-phase loading. Fatigue Eng Mate Struct, 11(3) (1988) 149–165.

[8] Itoh, T., Sakane, M., Ohnami, M., Socie, D.F., Non-proportional low cycle fatigue criterion for type 304 stainless steel. Trans Am Soc Mech Eng – J Eng Mater Technol, 117(3) (1995) 285–292.

[9] Chen, X., Gao, Q., Sun, X.F., Low-cycle fatigue under non-proportional loading. Fatigue Eng Mater Struct, 19(7) (1996) 839–854.

[10] Itoh, T., Nakata, T., Sakane, M., Ohnami, M., Non-proportional low cycle fatigue of 6061 aluminum alloy under 14 strain path. In: Macha et al., editors. Multiaxial Fatigue and Fracture, Vol. 25. Elsevier International Series on Structural Integrity, (1999) 41–54.

[11] Socie, D.F., Marquis, G.B., Multiaxial fatigue. SAE Int, (2000).

[12] Itoh, T., Effect of direction change in maximum principal strain axis on multiaxial low cycle fatigue life of type 304 stainless steel at elevated temperature. J Soc Mater Sci Jpn, 49(9) (2000) 988–993.

[13] Itoh, T., A model for evaluation of low cycle fatigue lives under non-proportional straining. J Soc Mater Sci, 50(12) (2001) 1317–1322.

[14] Chen, X., An, K., Kim, K.S., Low-cycle fatigue of 1Cr-18Ni-9Ti stainless steel and related weld metal under axial, torsional and 90°out-of-phase loading. Fatigue Eng Mater Struct, 27(6) (2004) 439–448.

[15] Shamsaei, N., Gladskyi, M., Panasovskyi, K., Shukaev, S., Fatemi, A., Multiaxial fatigue of titanium including step loading and load path alteration and sequence effects. Int J Fatigue, 32(11) (2010) 1862-1874.

[16] Itoh, T., Yang, T., Material dependence of multiaxial low cycle fatigue lives under non-proportional loading. Int J Fatigue, 33(8) (2011) 1025–1031.

[17] Kallmeyer, A.R., Krgo, A., Kurath, P., Evaluation of multiaxial fatigue life prediction methodologies for Ti-6Al-4V. Trans Am Soc Mech Eng – J Eng Mater Technol, 124(2) (2002) 229–237.

[18] Mall, S., Namjoshi, S.A., Porter, W.J., Effects of microstructure on fretting fatigue crack initiation behavior of Ti-6Al-4V. Materials Science and Engineering A, 383(2) (2004) 334-340.

[19] Nakamura, H., Takanashi, M., Itoh, T., Wu, M., Shimizu, Y., Fatigue Crack Initiation and Growth Behavior of Ti-6Al-4V under Non-Proportional Multiaxial Loading, 33(7) (2011) 842-848.

[20] Findley, W.N., Modified theory of fatigue failure under combined stress. In: Proc society experimental stress analysis, 14 (1956) 35–46.

[21] McDiarmid, D.L., A shear stress based critical plane criterion of multiaxial fatigue failure for design and life prediction. Fatigue Fract Eng Mater Struct, 17(12) (1994) 1475–1484.

[22] Brown, M.W., Miller, K.J., A theory for fatigue under multiaxial stress-strain conditions. In: Proc institution of mechanical engineering, 187 (1973) 745–756.

[23] Brown, M.W., Wang, C.H., A path-independent parameter for fatigue under proportional and non-proportional loading. Fatigue Fract Eng Mater Struct, 16(12) (1993) 1285-1298.

[24] Smith, R.N., Watson, P.P., Topper, T.H., A stress-strain parameter for the fatigue of metals. J Materials, 5(4) (1970) 767–778.

[25] Ogata, T., Nitta, A., Evaluation of multiaxial low-cycle fatigue failure based on new criterion and its application to high temperature structural design. Japan: Journal of the Society of Materials Science, 42 (1993) 77–72.